Geophysical Research Letters

RESEARCH LETTER
10.1029/2019GL082195

Cohesion-Induced Enhancement of Aeolian Saltation

F. Comola[1,2], J. Gaume[1,3], J. F. Kok[2], and M. Lehning[1,3]

[1]School of Architecture, Civil, and Environmental Engineering, Swiss Federal Institute of Technology, Lausanne, Switzerland, [2]Department of Atmospheric and Oceanic Sciences, University of California, Los Angeles, CA, USA, [3]WSL Institute for Snow and Avalanche Research, SLF, Davos, Switzerland

Abstract The wind-driven saltation of granular material plays a key role in various geophysical processes on Earth, Mars, Venus, and Titan. Although interparticle cohesion is known to limit the number of grains lifted from the surface through aerodynamic entrainment and granular splash, the role of cohesion in the development of saltation from onset to steady state is still poorly understood. Using a numerical model based on the discrete element method, we show that saltation over cohesive beds sustains itself at wind speeds 1 order of magnitude smaller than those necessary to initiate it, giving rise to hysteresis in which the occurrence of transport depends on the history of the wind. Our results further suggest that saltation over cohesive beds requires much longer distances to saturate, thereby increasing the size of the smallest stable bed forms. These findings have implications for dune formation, dust emission, and snow sublimation over cohesive beds.

Key Points:
- Saltation over cohesive surfaces requires high wind speed to initiate but much lower wind speed to sustain itself
- Saltation over cohesive surfaces saturates over long distances but presents high values of saturated mass flux
- Bed cohesion causes hysteresis in saltation and increases the size of the smallest stable bed forms

Supporting Information:
- Supporting Information S1

Correspondence to:
F. Comola,
francesco.comola@gmail.com

Citation:
Comola, F., Gaume, J., Kok, J. F., & Lehning, M. (2019). Cohesion-induced enhancement of aeolian saltation. *Geophysical Research Letters*, *46*, 5566–5574. https://doi.org/10.1029/2019GL082195

Received 24 JAN 2019
Accepted 22 APR 2019
Accepted article online 29 APR 2019
Published online 21 MAY 2019

1. Introduction

The wind-driven transport of granular materials, such as sand and snow, is ubiquitous in nature. In arid regions, windblown sand shapes dunes and ripples (Charru et al., 2013), erodes rocks to produce soils over long time periods (Pye, 2015), and triggers dust storms that travel halfway round the globe providing nutrients to several ecosystems (Jickells et al., 2005). This not only happens on Earth, where deserts cover one third of the land surface, but also on Mars, Venus, and Titan (Greeley & Iversen, 1985). In Antarctica, strong snow drift events erode and sublimate a significant amount of snow from the ice sheet (Scarchilli et al., 2010), causing a net loss in the surface mass balance and contributing to sea level rise. Our ability to quantify and predict these processes is still impaired by a limited understanding of the fundamental controls on sand and snow transport, in particular, as affected by the cohesion of the granular bed. Snow and wet sand grains, in fact, develop strong cohesive forces in form of sintered ice bonds (Schmidt, 1980) and water menisci (Ravi et al., 2004).

When wind blows over sand and snow surfaces, particles are lifted through aerodynamic entrainment and accelerated by the wind (Diplas et al., 2008). Airborne grains follow ballistic trajectories, reaching elevations of a few centimeters and subsequently impacting the granular bed. Upon collision, grains may then rebound or deposit depending on their speed and surface characteristics at the location of impact. Moreover, part of the impact kinetic energy is transferred to the granular bed. A fraction of this energy is used to eject other particles, typically from 1 to 10, through granular splash, while the remaining part is dissipated in frictional rearrangements and breaking of cohesive bonds between bed grains. At the onset, aerodynamic and splash entrainments dominate over deposition rate, leading to an increase in particle concentration and saltation mass flux. Simultaneously, the shear stress close to the surface drops as a significant amount of momentum is spent to accelerate the airborne grains (Anderson & Haff, 1988; Walter et al., 2014). A steady state is reached when the wind shear stress at the surface attains the minimum value at which saltation can be sustained, the so-called impact threshold (Bagnold, 1941; Martin & Kok, 2018). This complex series of near-surface flow-particle interactions is known as saltation (Anderson, 1989; Kok et al., 2012).

Starting from the seminal works of Bagnold (1941) and Owen (1964), our understanding of saltation transport mechanisms has advanced through experimental investigations (e.g., Mitha et al., 1986; Nalpanis et al., 1993; Rice et al., 1995), numerical simulations (e.g., Anderson & Haff, 1988; Durán et al., 2014; Kok & Renno, 2009), and theoretical models (e.g., Andreotti, 2004; Doorschot & Lehning, 2002; Pähtz et al., 2012). Despite the significant improvements in our understanding of saltation physics, the role played by interparticle cohesion remains largely unexplored. It is known that cohesion increases the threshold wind shear for

aerodynamic entrainment, the so-called fluid threshold (McKenna Neuman & Sanderson, 2008; Schmidt, 1980), and the impact energy necessary to splash grains from the surface (Comola & Lehning, 2017), overall limiting the number of particles in saltation. However, the role of surface cohesion in setting the development of saltation from the onset to steady state has remained poorly understood.

Here, we aim to shed light into the evolution of saltation over cohesive surfaces. Because it is extremely challenging to control bed cohesion in natural environments and even in wind tunnels, we use a numerical model based on the discrete element method (DEM). We first apply the model to study the role of cohesion in the granular splash process, which is the main entrainment mechanism in steady state saltation. We then perform simulations of the overall saltation process to investigate the evolution of saltation mass flux and surface wind shear over cohesive surfaces. A deeper insight into the saltation dynamics of cohesive granular materials may lead to more accurate quantifications of large-scale environmental processes in arid and polar regions.

2. Saltation Model

We integrate the equations of motion of particles subject to gravity forces, aerodynamic forces, interparticle collisions, and cohesive forces. For the generic particle of mass m, moment of inertia $\mathbf{J}$, velocity vector $\mathbf{V}$, and rotational spin vector ω, the equations of motion read

$$m\frac{\mathrm{d}\mathbf{V}}{\mathrm{d}t} = \sum \mathbf{F} - \mathbf{g}, \quad \mathbf{J}\frac{\mathrm{d}\boldsymbol{\omega}}{\mathrm{d}t} = \sum \mathbf{R}. \tag{1}$$

In equation (1), $\sum \mathbf{F}$ indicates the sum of collisional forces and aerodynamic forces acting on the particle, $\sum \mathbf{R}$ the sum of all rotational forces, and $\mathbf{g} = (0, 0, g)$ is the gravitational force. The time integration of equation (1) is performed with a second-order accurate Verlet scheme (Verlet, 1967).

When two particles are in contact, either as a result of a collision or because they rest one on the other, normal forces $\mathbf{F}_n$ and shear forces $\mathbf{F}_s$ at the contact point are simulated with the DEM model PFC3D (Itasca Consulting Group, 2014), which implements the viscoelastic model of Cundall and Strack (1979). The elastic component is envisioned as a linear spring with constant normal and shear stiffnesses k_n and k_s, while the viscous contribution is generated by a dashpot model with damping coefficients ν_n and ν_s (Akyildiz et al., 1990), that is,

$$\mathbf{F}_n = -k_n\boldsymbol{\delta}_n - \nu_n\dot{\boldsymbol{\delta}}_n, \quad \mathbf{F}_s = -k_s\boldsymbol{\delta}_s - \nu_s\dot{\boldsymbol{\delta}}_s. \tag{2}$$

In equation (2), $\delta_n > 0$ is the particle interpenetration, $\dot{\boldsymbol{\delta}}_n$ is the interpenetration velocity, δ_s is the relative tangential displacement accumulated during the slip, and $\dot{\boldsymbol{\delta}}_s$ is the slip velocity. The normal stiffness $k_n = \pi dE/4$ is a function of the elastic modulus E and the particle diameter d, while the shear stiffness $k_s = k_n/k^*$ is proportional to the normal stiffness through the constant ratio k^*. If k_n and k_s are large, as is typically the case for windblown sediments, particle interpenetration and slip are small. However, if the shear force exceeds the Coulombian threshold $\mu|\mathbf{F}_n|$, significant relative slip takes place under constant shear force $\mathbf{F}_s = \mu|\mathbf{F}_n|$.

When particles are bonded, as is the case for neighboring elements at the onset of the simulation, the standard contact model is modified to include additional tensile and shear strengths (Potyondy & Cundall, 2004). Accordingly, the elastic spring of equation (2) works also in extension for $\delta_n < 0$. We define cohesion F_ϕ as the maximum tensile or shear force that the bond can sustain before breaking. As long as $\mathbf{F}_n < F_\phi$ and $\mathbf{F}_s < F_\phi$, significant relative displacement and slip between the particles are suppressed. Conversely, if the bond breaks either in tension or in shear, the standard contact model is resumed. This type of bonded contact model was previously adopted to study snowflake fragmentation (Comola et al., 2017) and snow fracture (Gaume et al., 2017).

Particles splashed from the granular bed into the turbulent flow are subjected to aerodynamic drag and lift forces. The drag force $\mathbf{F}_d$ is proportional to the velocity difference between the flow and the particle, while the vertical lift force F_l is proportional to the flow velocity difference between the upper and lower sides of the particle (Carneiro et al., 2011), that is,

$$\mathbf{F}_d = \frac{1}{2}\rho_f C_d A|\mathbf{U} - \mathbf{V}|(\mathbf{U} - \mathbf{V}), \quad F_l = \frac{\pi d^3}{8}\rho_f C_l \nabla\left(U_x - V_x\right)^2. \tag{3}$$

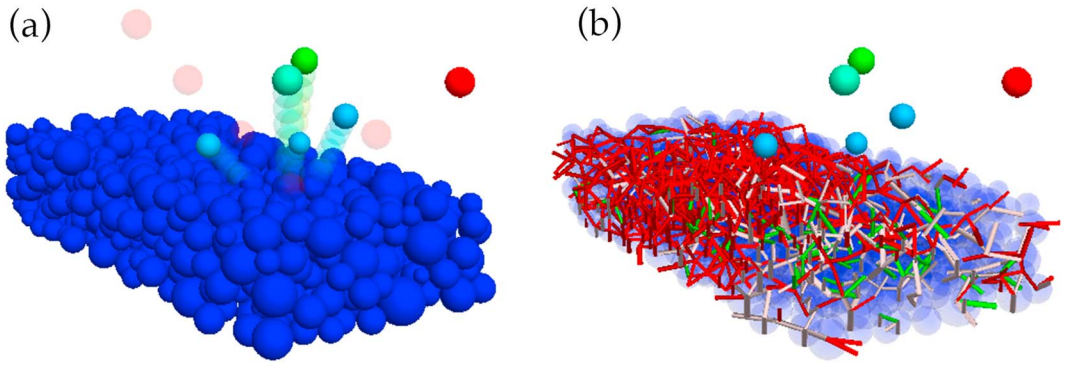

Figure 1. Representation of the model simulations to study the effect of cohesion on the granular splash process. (a) A high-speed grain (red sphere) impacts the granular bed, rebounds, and splashes other grains with small liftoff velocities (green and light blue spheres). (b) Breaking of cohesive bonds upon the same splash event. In the vicinity of the impact location, some of the cohesive bonds (red beams) break in tension (white beams) while others break in shear (green beams).

$\mathbf{U}$ is the wind velocity vector, ρ_f is the fluid density, and $\mathbf{V}$ the particle velocity vector. Further, $A = \pi/4d^2$ is the particle cross-sectional area, C_d is the drag coefficient for natural sediments proposed by Cheng (1997; see supporting information Text S1.1), and $C_l \approx 0.4C_d$ is the lift coefficient (Chepil, 1958).

The wind field $\mathbf{U} = \left(U_x, 0, u_z\right)$ is characterized by a mean streamwise component U_x and turbulent fluctuations u_z in the vertical direction. We compute U_x with a modified law of the wall (Kok et al., 2012)

$$\frac{\mathrm{d}U_x}{\mathrm{d}z} = \frac{u_*}{k\,(z-h)}\left(1 - \frac{\tau_p(z)}{\rho_f u_*^2}\right), \tag{4}$$

where u_* is the assigned shear velocity outside of the saltation layer, $k \approx 0.4$ is the von Kármán constant, and h is the time-dependent bed height (see equation (S4) in the supporting information). Further, $\tau_p(z)$ is the particle shear stress that accounts for the wind momentum spent to accelerate particles. Following numerical implementations of previous studies (e.g., Carneiro et al., 2011, 2013; Durán et al., 2012), we calculate $\tau_p(z)$ by integration of the drag forces acting on airborne particles at elevations larger than z (see equation (S2) in the supporting information). The initial wind profile corresponds to the analytical solution of equation (4) in the absence of airborne particles ($\tau_p = 0$), that is, the well-known logarithmic law of the wall over aerodynamically rough surfaces (Keulegan, 1938; Nikuradse, 1933; Prandtl, 1952; see equation (S3) in the supporting information).

The vertical velocity fluctuations u_z are calculated with the Lagrangian stochastic model proposed by Wilson & Sawford (1996; see supporting information Text S1.3).

A similar description of the wind field was adopted and tested in several previous DEM models of saltation (e.g., Carneiro et al., 2011, 2013; Pähtz et al., 2015) and allows for an effective description of the fundamental flow-particle interactions at the small scales of interest. We further verify that our model is able to reproduce with sufficient accuracy the granular splash (Gordon & McKenna-Neuman, 2011; Rice et al., 1995, 1996; Willetts & Rice, 1985, 1986, 1989) and saltation dynamics (Andreotti et al., 2010; Martin & Kok, 2018; Walter et al., 2014) of loose sand (supporting information Texts S2 and S3) and feel thus confident to further apply the tested model setup to investigate the role of cohesion.

3. Granular Splash Simulations

We start our analysis by studying the effect of cohesion on the granular splash process, which is the most efficient entrainment mechanism in saltation. The predisposition to fracture of the cohesive bed upon impact of a saltating grain is characterized by the fragmentation number (Rognon et al., 2008; Steinkogler et al., 2015)

$$\eta_f = \frac{\sqrt{\langle m\rangle\langle k_n\rangle}\langle V_i\rangle}{F_\phi}. \tag{5}$$

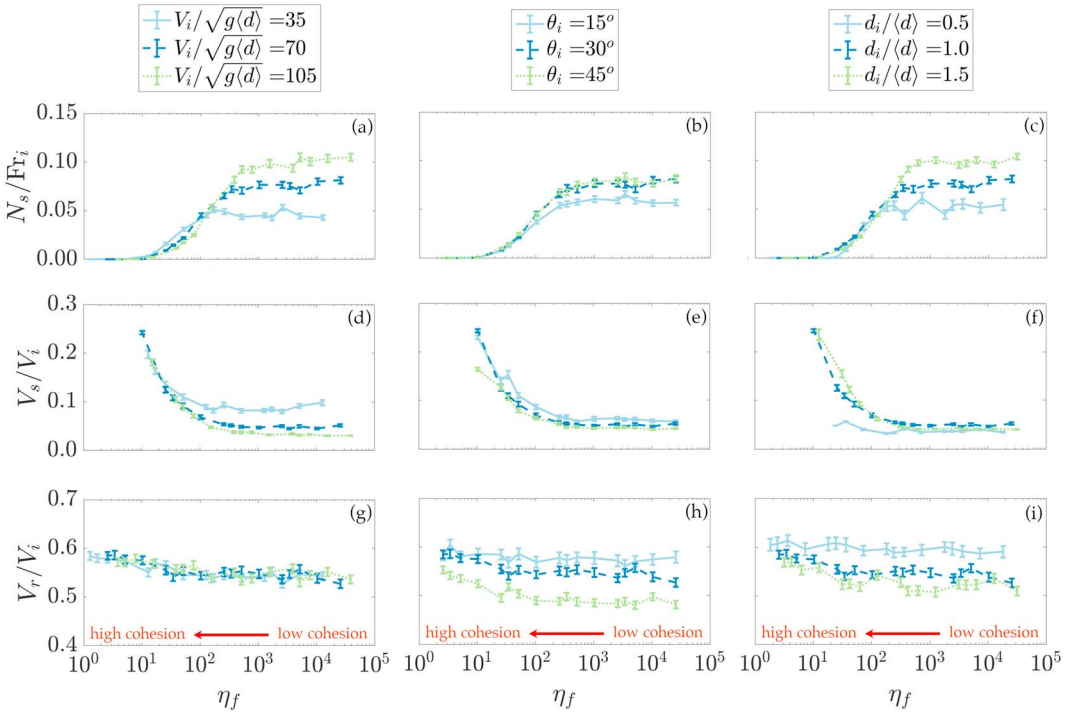

Figure 2. (a–c) Number of splashed particles N_s as a function of the fragmentation number η_f (equation (5)), for different values of (a) impact velocity V_i, (b) impact angle θ_i, and (c) impactor size d_i. Values are normalized by the impact Froude number $\mathrm{Fr}_i = m_i V_i/\langle m\rangle\sqrt{g\langle d\rangle}$, where m_i is the mass of the impactor and $\langle m\rangle$ is the mean particle mass. (d–f) Ratio of splash velocity V_s over impact velocity V_i for different values of (d) impact velocity, (e) impact angle, and (f) impactor size. (g–i) Ratio of rebound restitution coefficient V_r/V_i for different values of (g) impact velocity, (h) impact angle, and (i) impactor size. When testing the sensitivity to one parameter, the other parameters are kept at their reference values ($V_i/\sqrt{g\langle d\rangle} = 70$, $\theta_i = 30°$, and $d_i/\langle d\rangle = 1$). Lines interpolate mean values and vertical bars indicate standard errors.

In equation (5), $\langle m\rangle$ indicates the mean particle mass, $\langle k_n\rangle$ the mean normal stiffness of particle contacts, and $\langle V_i\rangle$ the mean particle impact velocity. The fragmentation number represents the ratio between the impact energy $\langle m\rangle V_i^2/2$ and the elastic energy of the bonds at the fracture limit $F_\phi^2/2\langle k_n\rangle$. We assign the size d_i, velocity V_i, and direction θ_i of the impacting grain and conventionally identify the splashed grains as those particles that reach an elevation above the surface equal to one mean diameter (Crassous et al., 2007). Because aerodynamic forces have negligible effects on the granular splash process (Haff & Anderson, 1993), we perform simulations in absence of background wind.

We consider snow grain properties by assigning $\rho_p = 910\,\mathrm{kg/m^3}$ and d with lognormal distribution of mean value $\langle d\rangle = 200\,\mu\mathrm{m}$ and standard deviation $\sigma_d = 50\,\mu\mathrm{m}$ (see supporting information Text S2 for additional details on the model parameters; Haff & Anderson, 1993). We investigate a wide range of cohesion values F_ϕ within 10^{-7}–10^{-3} N. Note that the lower limit corresponds to sand and powder snow cohesion, while the upper limit corresponds to sintered snow cohesion (see, e.g., Schmidt, 1980; Shao & Lu, 2000, and references therein). The dimensions of the computational domain are $L_x = 20\langle d\rangle$ and $L_y = 10\langle d\rangle$, with periodic boundary conditions in the x and y directions. The granular bed has a porosity $p \approx 0.6$ and mean height $h \approx 12\langle d\rangle$, which is sufficient to suppress the reflection of shock waves at the lower boundary of the computational domain (Carneiro et al., 2013; Rioual et al., 2000). A representation of our granular splash simulations is shown in Figure 1.

The results indicate an increase in the number of splashed grains N_s with η_f (Figures 2a–2c) confirming the well-known cohesion-induced supply limitation of particles to the saltation process. The number of splashed grains is sensitive to the velocity V_i and size d_i of the impacting grain (Figures 2a and 2c), which regulate the energy and momentum transferred to the bed upon collision. Conversely, the average velocity of the splashed grains V_s (Figures 2d–2f) shows a visible decrease with η_f, with significant sensitivity only to the impact velocity (Figure 2d). The simulations further indicate that the increase in V_s sustains the total

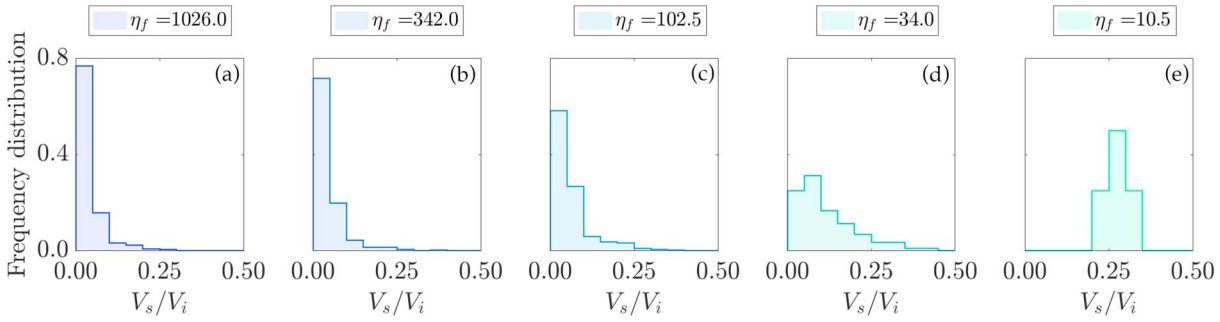

Figure 3. Velocity distributions of splashed grains for decreasing values of the fragmentation number η_f, from a nearly loose granular bed (a) to a highly cohesive granular bed (e). With increasing cohesion, the distribution peak lowers (b, c) and shifts toward larger values (d, e). These results are obtained for assigned impact velocity $V_i/\sqrt{g\langle d\rangle} = 70$, impact angle $\theta_i = 30°$, and impactor size $d_i = \langle d\rangle$. The mean values of these distributions correspond to the blue data points in Figures 2d–2f.

kinetic energy of splashed grains across the tested range of cohesion, as the larger liftoff velocity compensates for the smaller number of ejecta (see supporting information Text S4.1). In addition to the splash velocity, cohesion also increases the restitution coefficient of the rebounding grain (Figures 2g–2i), as a result of the larger elasticity of cohesive beds.

We provide a deeper insight into the variation of splash velocity with cohesion by computing the frequency distributions of ejection velocity for assigned values of impact velocity $V_i/\sqrt{g\langle d\rangle} = 70$, impact angle $\theta_i = 30°$, and impactor size $d_i = \langle d\rangle$. For nearly cohesionless granular beds (Figure 3a), the probability distribution peaks at $V_s < 0.05V_i$ and shows a sharp decrease for larger values, consistently with results of previous studies (see, e.g., Beladjine et al., 2007; Mitha et al., 1986). At higher cohesion (Figures 3b–3d), the peak lowers and shifts toward larger values of splash velocity. For highly cohesive beds (Figure 3e), the frequency distribution peaks at $V_s \approx 0.3V_i$, with almost no occurrence for $V_s < 0.2V_i$. We perform a similar analysis on the frequency distribution of the rebound velocity and observe a smaller yet significant sensitivity to the surface cohesion (see supporting information Text S4.2).

We argue that the reason for the decrease in splash velocity with fragmentation number lies in the fundamentally different mechanisms that drive granular splash in cohesive beds with respect to loose beds. While loose grains are essentially splashed through a chain of binary particle collisions (Crassous et al., 2007), cohesive grains are splashed through unbalanced forces generated by breaking of interparticle bonds. Given that large cohesion generates large unbalanced forces, splashed grains experience on average larger accelerations (see supporting information Text S4.3 for analyses and additional details). This splash mechanism is analogous to a tug of war where two players (two grains) pull a rope (the cohesive bond) with equivalent forces: the players are more likely to snap a thin rope (low cohesion) but experience a stronger recoil if they snap a thick rope (high cohesion).

4. Saltation Simulations

It is known that saltation reaches stationarity when the mean replacement capacity is equal to one, that is, when every impacting grain that fails to rebound is replaced by one splashed grain (Bagnold, 1941; Kok et al., 2012). The particle supply limitation caused by cohesion implies that, on average, particles in saltation must impact the granular bed at higher speed to keep the particle concentration stationary. This is likely to require a higher near-surface wind speed, that is, higher impact threshold compared to saltation over loose granular beds. We argue, however, that the cohesion-induced enhancement of splash velocity and restitution coefficient may fundamentally promote higher particle velocities, preventing a significant increase in the impact threshold.

To evaluate this hypothesis, we carry out model simulations of the whole saltation process. We increase the size of the computational domain to $L_x = 700\langle d\rangle$ and $L_y = 40\langle d\rangle$, with periodic boundary conditions for particle positions. We perform simulations for different values of η_f, triggering saltation by granular splash of a single grain at the inlet section ($x = 0$) and letting the system evolve until saltation reaches a stationary condition. We assign air density $\rho_f = 1.2\,\mathrm{kg/m^3}$ and initial shear velocity $u_* = 0.25\,m/s$. We estimate the fragmentation number η_f of the saltation cloud using a modified version equation (5), where the impact velocity V_i is replaced by the mean velocity of the saltating particles.

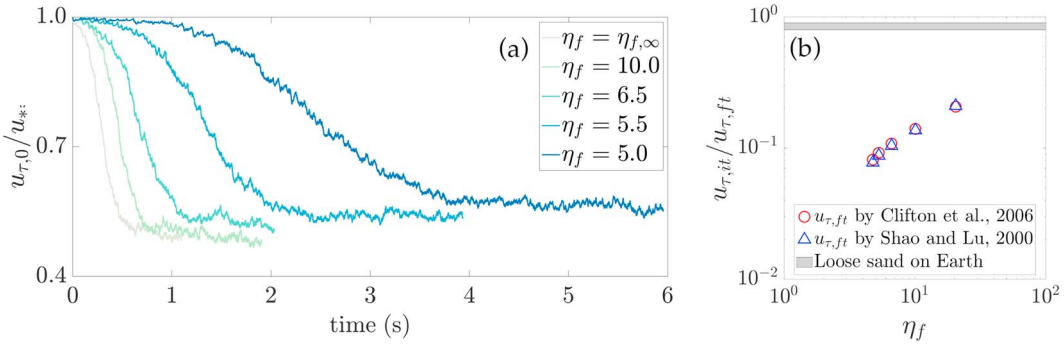

Figure 4. (a) Time series of near-surface wind shear velocity $u_{\tau,0}$, normalized by the assigned shear velocity outside of the saltation layer u_*. (b) Separation between impact threshold $u_{\tau,it}$ and fluid threshold $u_{\tau,ft}$ for different values of fragmentation number. The impact threshold is estimated from our saltation simulations, while the fluid threshold is calculated with equations proposed by Clifton et al. (2006) and Shao and Lu (2000; see supporting information Text S4.4 for additional details).

The time series of near-surface shear velocity $u_{\tau,0}$ (Figure 4a) present an initial decrease, as particles are entrained and accelerated by the wind, and a subsequent relaxation toward the impact threshold $u_{\tau,it}$. The results suggest that, in the presence of cohesion, saturated saltation presents impact thresholds slightly higher than the cohesionless case ($\eta_f = \eta_{f,\infty}$ in the figure's legend). This increase of impact threshold with cohesion, however, is significantly smaller than the cohesion-induced increase in the fluid threshold suggested by previous studies (Clifton et al., 2006; Shao & Lu, 2000). The separation between fluid and impact thresholds is of primary importance in aeolian transport as it controls the difference in wind speed necessary to initiate and to sustain saltation (Kok, 2010). We estimate the effect of cohesion on the separation between fluid and impact thresholds using the formulations of $u_{\tau,ft}$ proposed by Clifton et al. (2006) and Shao and Lu (2000; see supporting information Text S4.4 for the additional details). The results (Figure 4b) suggest that for small values of the fragmentation number the ratio between impact and fluid threshold is one order of magnitude smaller than the reference range 0.80–0.86 (gray area in Figure 4b) measured for saltation of loose sand on Earth (Martin & Kok, 2018; Walter et al., 2014).

We further show the effect of cohesion on the evolution of saltation mass flux $Q = \sum_k^N m_k V_{x,k}/L_x L_y$ (Figure 5a). All mass flux time series present an initial increase and a relaxation phase toward the saturated values. For decreasing values of η_f, saltation mass flux requires an increasingly longer time to saturate but presents larger values of saturated mass flux Q_s due to the increase in particle velocity (see supporting information Text S4.5 for particle concentration time series). The distance needed for the flux to adapt to a change in flow conditions, known as saturation length L_s, is a fundamental control on aeolian transport as it critically affects dune dynamics by setting the minimum length scale over which a dune is stable against erosion (Pähtz et al., 2013). We can estimate L_s using the analytical expression of the mass flux relaxation

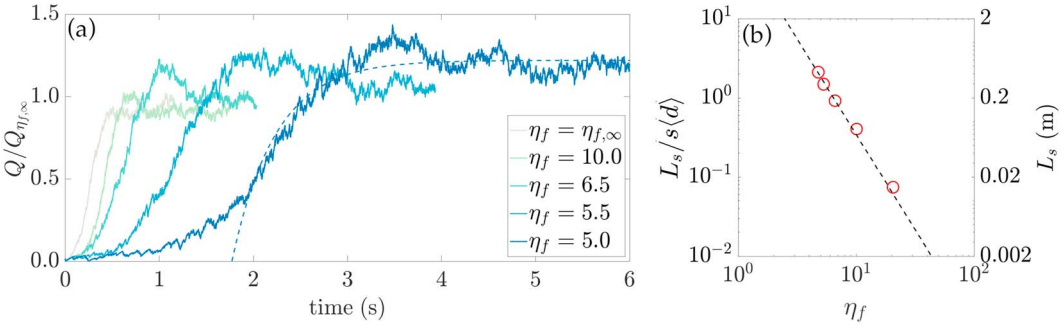

Figure 5. (a) Time series of saltation mass flux, normalized by the reference mass flux $Q_{\eta_f,\infty}$, corresponding to the saturated mass flux over a loose granular bed. The dashed line is an example of the analytical solution (equation (6)) fitted to the model time series. (b) Variation in the flux saturation length L_s with the fragmentation number. On the left axis, the saturation length is normalized by the density ratio $s = \rho_p/\rho_f$ and mean grain diameter $\langle d\rangle$. The red circles indicate numerical results and the dashed line indicates the best fit power law scaling.

toward the saturated value Q_s (Pähtz et al., 2015)

$$\frac{Q}{Q_s} = 1 - \exp\left(-\frac{\int_0^t V_p \mathrm{d}t' - x_0}{L_s}\right), \tag{6}$$

where V_p is the average velocity of the saltation cloud and x_0 is an integration constant. By fitting Q_s, x_0, and L_s of equation (6) to our saltation simulations (see an example in Figure 5a), we find that saturation length scales like a power law of the fragmentation number (Figure 5b), with a significant variation of almost 2 orders of magnitude within the tested range of cohesion.

5. Conclusions

When wind blows over a granular bed, particles are entrained in the flow and follow stretched ballistic trajectories close to the surface. This process, known as saltation, is sustained primarily through granular splash, that is, the ejection of surface grains upon impact of other windblown particles with the bed. The granular splash process is highly stochastic, as it depends on size and velocity of the impacting grain and on the bed properties at the impact location. Among these properties, interparticle cohesion is one of the most influential and yet one of the most unexplored controls.

Here, we applied a model based on the DEM to provide a deeper insight into the role of particle cohesion in saltation of granular materials. Model results indicate a twofold effect of cohesion on granular splash: it decreases the number of splashed grains, while increasing the velocity of the splashed particles and the restitution coefficient of the rebounding grain. The reasons for the increase in splash velocity seem to lie in the peculiar ejection mechanics from cohesive beds, which is due to unbalanced forces generated upon breaking of interparticle bonds.

We further performed simulations of the full saltation process to show that the wind speed necessary to sustain saltation over cohesive beds is much (by approximately tenfold) lower than that necessary to initiate it. This is likely a consequence of the cohesion-induced enhancement of splash velocity and restitution coefficient, which sustain a faster saltation. This suggests that the occurrence of saltation at wind speeds between the impact and fluid thresholds depends on the history of the system, a phenomenon known as hysteresis.

Furthermore, model results indicate that saltation over cohesive surfaces requires much longer distances to saturate. This is likely a consequence of the increase in particle speed required for saltation to attain a mean replacement capacity equal to one. In other words, saltating grains over cohesive beds require several more hop lengths to reach an impact velocity that produces on average one new splashed particle for each grain that fails to rebound. We quantified the cohesion-induced retardation of saltation by calculating the flux saturation lengths from our simulations, which present a power law scaling with bed cohesion and variations of 2 orders of magnitude in the tested range of cohesion. The increase in saturation length suggests that the size of the smallest stable bed forms may be significantly larger on snow surfaces than on loose sand surfaces.

Our findings may have important implications for large-scale aeolian processes. The identification of cohesion as a fundamental control on flux saturation length may help to shed light on the morphodynamics of snow dunes. Moreover, the cohesion-induced enhancement of saltation fluxes and the occurrence of hysteresis may have implications for dust emission from soils with cohesive crusts, blowing-snow sublimation over snow surfaces, and aeolian transport on Titan, where tholin grains formed of solid methane are thought to be very cohesive.

Acknowledgments
F. C., J. G., and M. L. acknowledge the financial support by the Swiss National Science Foundation (projects PZ00P2_142684, P2ELP2_178219, and PCEFP2_181227). J. F. K. acknowledges the financial support by the NASA Outer Planets Research grant 131186, and by the Army Research Laboratory grant W911NF-15-1-0417. The authors are grateful to Mark Gordon and Cheryl McKenna-Neuman for providing experimental data and for the insightful discussions. The author further wish to thank Robert S. Anderson for his constructive comments on the manuscript. All data presented in this paper are publicly accessible at the EnviDat data portal (https://www.envidat.ch/dataset/saltation-of-cohesive-granular-materials).

References

Akyildiz, F., Jones, R. S., & Walters, K. (1990). On the spring-dashpot representation of linear viscoelastic behaviour. *Rheologica Acta*, *29*(5), 482–484.

Anderson, R. S. (1989). Saltation of sand: A qualitative review with biological analogy. *Proceedings of the Royal Society of Edinburgh, Section B: Biological Sciences*, *96*, 149–165.

Anderson, R. S., & Haff, P. K. (1988). Simulation of eolian saltation. *Science*, *241*(4867), 820–823.

Andreotti, B. (2004). A two-species model of aeolian sand transport. *Journal of Fluid Mechanics*, *510*, 47–70.

Andreotti, B., Claudin, P., & Pouliquen, O. (2010). Measurements of the aeolian sand transport saturation length. *Geomorphology*, *123*(3–4), 343–348.

Bagnold, R. A. (1941). *The physics of blown sand and desert dunes*. London: Methuen.

Beladjine, D., Ammi, M., Oger, L., & Valance, A. (2007). Collision process between an incident bead and a three-dimensional granular packing. *Physical Review E*, *75*(6), 61305.
Carneiro, M. V., Araújo, N. A. M., Pähtz, T., & Herrmann, H. J. (2013). Midair collisions enhance saltation. *Physical Review Letters*, *111*(5), 58001.
Carneiro, M. V., Pähtz, T., & Herrmann, H. J. (2011). Jump at the onset of saltation. *Physical Review Letters*, *107*, 98001.
Charru, F., Andreotti, B., & Claudin, P. (2013). Sand ripples and dunes. *Annual Review of Fluid Mechanics*, *45*, 469–493.
Cheng, N. S. (1997). Simplified settling velocity formula for sediment particle. *Journal of Hydraulic Engineering*, *123*(2), 149–152.
Chepil, W. S. (1958). The use of evenly spaced hemispheres to evaluate aerodynamic forces on a soil surface. *Transactions of the American Geophysical Union*, *39*(3), 397–404.
Clifton, A., Rüedi, J., & Lehning, M. (2006). Snow saltation threshold measurements in a drifting-snow wind tunnel. *Journal of Glaciology*, *52*(179), 585–596.
Comola, F., Kok, J. F., Gaume, J., Paterna, E., & Lehning, M. (2017). Fragmentation of wind-blown snow crystals. *Geophysical Research Letters*, *44*, 4195–4203. https://doi.org/10.1002/2017GL073039
Comola, F., & Lehning, M. (2017). Energy- and momentum-conserving model of splash entrainment in sand and snow saltation. *Geophysical Research Letters*, *44*, 1601–1609. https://doi.org/10.1002/2016GL071822
Crassous, J., Beladjine, D., & Valance, A. (2007). Impact of a projectile on a granular medium described by a collision model. *Physical Review Letters*, *99*(24), 248001.
Cundall, P. A., & Strack, O. D. L. (1979). A discrete numerical model for granular assemblies. *Géotechnique*, *29*(1), 47–65.
Diplas, P., Dancey, C. L., Celik, A. O., Valyrakis, M., Greer, K., & Akar, T. (2008). The role of impulse on the initiation of particle movement under turbulent flow conditions. *Science*, *322*(5902), 717–720.
Doorschot, J. J. J., & Lehning, M. (2002). Equilibrium saltation: Mass fluxes, aerodynamic entrainment, and dependence on grain properties. *Boundary-Layer Meteorology*, *104*(1), 111–130.
Durán, O., Andreotti, B., & Claudin, P. (2012). Numerical simulation of turbulent sediment transport, from bed load to saltation. *Physics of Fluids*, *24*(10), 103306.
Durán, O., Claudin, P., & Andreotti, B. (2014). Direct numerical simulations of aeolian sand ripples. *Proceedings of the National Academy of Sciences of the United States of America*, *111*(44), 15,665–15,668.
Gaume, J., van Herwijnen, A., Chambon, G, Wever, N., & Schweizer, J. (2017). Snow fracture in relation to slab avalanche release: Critical state for the onset of crack propagation. *Cryosphere*, *11*(1), 217–228.
Gordon, M., & McKenna-Neuman, C. (2011). A study of particle splash on developing ripple forms for two bed materials. *Geomorphology*, *129*(1–2), 79–91.
Greeley, R., & Iversen, J. D. (1985). *Wind as a geological process: On Earth, Mars, Venus and Titan*. New York: Cambridge University Press.
Haff, P. K., & Anderson, R. S. (1993). Grain scale simulations of loose sedimentary beds: The example of grain-bed impacts in aeolian saltation. *Sedimentology*, *40*(2), 175–198.
Itasca Consulting Group (2014). PFC–Particle Flow Code, ver. 5.0 [Computer software manual].
Jickells, T. D., An, Z. S., Andersen, K. K., Baker, A. R., Bergametti, G., Brooks, N., et al. (2005). Global iron connections between desert dust, ocean biogeochemistry, and climate. *Science*, *308*(5718), 67–71.
Keulegan, G. H. (1938). *Laws of turbulent flow in open channels* (Vol. 21, pp. 707–741). Gaithersburg, MD: National Bureau of Standards US.
Kok, J. F. (2010). Difference in the wind speeds required for initiation versus continuation of sand transport on Mars: Implications for dunes and dust storms. *Physical Review Letters*, *104*(7), 74502.
Kok, J. F., Parteli, E. J. R., Michaels, T. I., & Karam, D. B. (2012). The physics of wind-blown sand and dust. *Reports on Progress in Physics*, *75*(10), 106901.
Kok, J. F., & Renno, N. O. (2009). A comprehensive numerical model of steady state saltation (COMSALT). *Journal of Geophysical Research*, *114*, D17204. https://doi.org/10.1029/2009JD011702
Martin, R. L., & Kok, J. F. (2018). Distinct thresholds for the initiation and cessation of aeolian saltation from field measurements. *Journal of Geophysical Research: Earth Surface*, *123*, 1546–1565. https://doi.org/10.1029/2017JF004416
McKenna Neuman, C., & Sanderson, S. (2008). Humidity control of particle emissions in aeolian systems. *Journal of Geophysical Research*, *113*, F02S14. https://doi.org/10.1029/2007JF000780
Mitha, S., Tran, M. Q., Werner, B. T., & Haff, P. K. (1986). The grain-bed impact process in aeolian saltation. *Acta Mechanica*, *63*(1–4), 267–278.
Nalpanis, P., Hunt, J. C. R., & Barrett, C. F. (1993). Saltating particles over flat beds. *Journal of Fluid Mechanics*, *251*, 661–685.
Nikuradse, J. (1933). Strömungsgesetze in rauhen Rohren. *VDI-Forschungsheft*, *361*, 1.
Owen, P. R. (1964). Saltation of uniform grains in air. *Journal of Fluid Mechanics*, *20*(2), 225–242.
Pähtz, T., Kok, J. F., & Herrmann, H. J. (2012). The apparent roughness of a sand surface blown by wind from an analytical model of saltation. *New Journal of Physics*, *14*(4), 43035.
Pähtz, T., Kok, J. F., Parteli, E. J. R., & Herrmann, H. J. (2013). Flux saturation length of sediment transport. *Physical Review Letters*, *111*(21), 218002.
Pähtz, T., Omeradžić, A., Carneiro, M. V., Araújo, N. A. M., & Herrmann, H. J. (2015). Discrete element method simulations of the saturation of aeolian sand transport. *Geophysical Research Letters*, *42*, 2063–2070. https://doi.org/10.1002/2014GL062945
Potyondy, D. O., & Cundall, P. A. (2004). A bonded-particle model for rock. *International Journal of Rock Mechanics and Mining Sciences*, *41*(8), 1329–1364.
Prandtl, L. (1952). *Essentials of fluid dynamics: With applications to hydraulics, aeronautics, meteorology, and other subjects*: New York: Hafner Publishing Company.
Pye, K. (2015). *Aeolian dust and dust deposits*. London, UK: Elsevier, Academic Press.
Ravi, S., D'Odorico, P., Over, T. M., & Zobeck, T. M. (2004). On the effect of air humidity on soil susceptibility to wind erosion: The case of air-dry soils. *Geophysical Research Letters*, *31*, L09501. https://doi.org/10.1029/2004GL019485
Rice, M. A., Willetts, B. B., & McEwan, I. K. (1995). An experimental study of multiple grain-size ejecta produced by collisions of saltating grains with a flat bed. *Sedimentology*, *42*(4), 695–706.
Rice, M. A., Willetts, B. B., & McEwan, I. K. (1996). Observations of collisions of saltating grains with a granular bed from high-speed cine-film. *Sedimentology*, *43*(1), 21–31.
Rioual, F., Valance, A., & Bideau, D. (2000). Experimental study of the collision process of a grain on a two-dimensional granular bed. *Physical Review E*, *62*(2), 2450.
Rognon, P. G., Chevoir, F., Bellot, H., Ousset, F., Naaïm, M., & Coussot, P. (2008). Rheology of dense snow flows: Inferences from steady state chute-flow experiments. *Journal of Rheology*, *52*(3), 729–748.

Scarchilli, C., Frezzotti, M., Grigioni, P., De Silvestri, L., Agnoletto, L., & Dolci, S. (2010). Extraordinary blowing snow transport events in East Antarctica. *Climate Dynamics*, *34*, 1195–1206.

Schmidt, R. A. (1980). Threshold wind-speeds and elastic impact in snow transport. *Journal of Glaciology*, *26*, 453–467.

Shao, Y., & Lu, H. (2000). A simple expression for wind erosion threshold friction velocity. *Journal of Geophysical Research*, *105*(D17), 22,437–22,443.

Steinkogler, W., Gaume, J., Löwe, H., Sovilla, B., & Lehning, M. (2015). Granulation of snow: From tumbler experiments to discrete element simulations. *Journal of Geophysical Research: Earth Surface*, *120*, 1107–1126. https://doi.org/10.1002/2014JF003294

Verlet, L. (1967). Computer "experiments" on classical fluids. I. Thermodynamical properties of Lennard-Jones molecules. *Physical Review*, *159*(1), 98.

Walter, B., Horender, S., Voegeli, C., & Lehning, M. (2014). Experimental assessment of Owen's second hypothesis on surface shear stress induced by a fluid during sediment saltation. *Geophysical Research Letters*, *41*, 6298–6305. https://doi.org/10.1002/2014GL061069

Willetts, B. B., & Rice, M. A. (1985). Inter-saltation collisions. In *Proc. int. workshop on physics of blown sand* (Vol. 1, pp. 83–100). Aarhus, Denmark.

Willetts, B. B., & Rice, M. A. (1986). Collisions in aeolian saltation. *Acta Mechanica*, *63*(1–4), 255–265.

Willetts, B. B., & Rice, M. A. (1989). Collisions of quartz grains with a sand bed: The influence of incident angle. *Earth Surface Processes and Landforms*, *14*(8), 719–730.

Wilson, J. D., & Sawford, B. L. (1996). Review of Lagrangian stochastic models for trajectories in the turbulent atmosphere. *Boundary-Layer Meteorology*, *78*(1), 191–210.